Supporting Information

Easily construct imine bonded COFs for iodine capture at ambient temperature

Yonghe Sun[a], Sanan Song[b], Dehai Xiao[c], Linfeng Gan[c*], Yuanrui Wang[a*]

a Academy of Chemical Engineering, Changchun University of technology, Changchun, Jilin 130012, China.

b College of Chemistry, Jilin University, Changchun, Jilin 130012, China.

c Changchun Institute of Applied Chemistry, Chinese Academy of Sciences, Changchun, Jilin 130022, China.

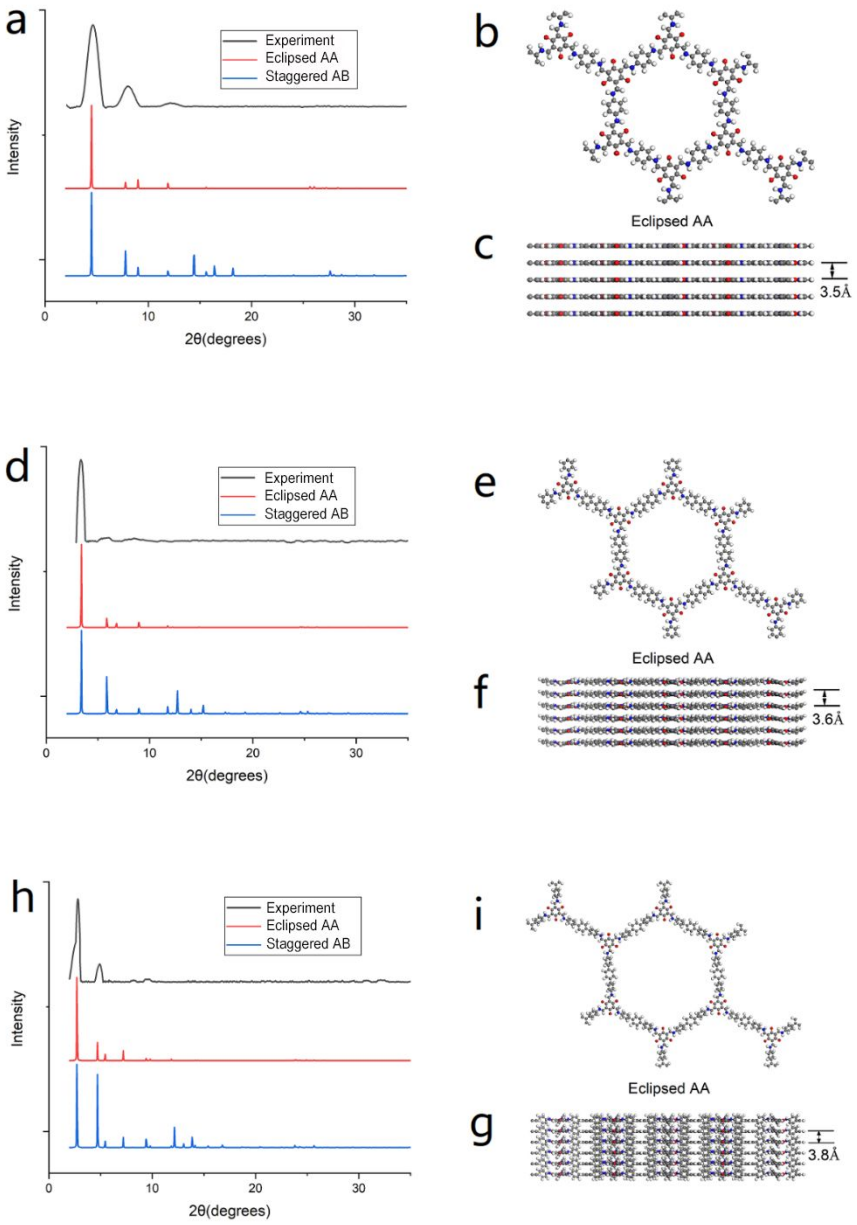

Figure S1. PXRD patterns (black, major reflections) and simulations (red and blue) profiles of **(a)** COF-TpgDB, **(b, c)** simulational eclipsed structure of COF-TpgDB, **(d)** PXRD patterns (black, major reflections) and simulations (red and blue) profiles of COF-TpgBD, **(e, f)** simulational eclipsed structure of COF-TpgBD, **(h)** PXRD patterns (black, major reflections) and simulations (red and blue) profiles of COF-TpgTd, **(i, g)** simulational eclipsed structure of COF-

TpgTd.

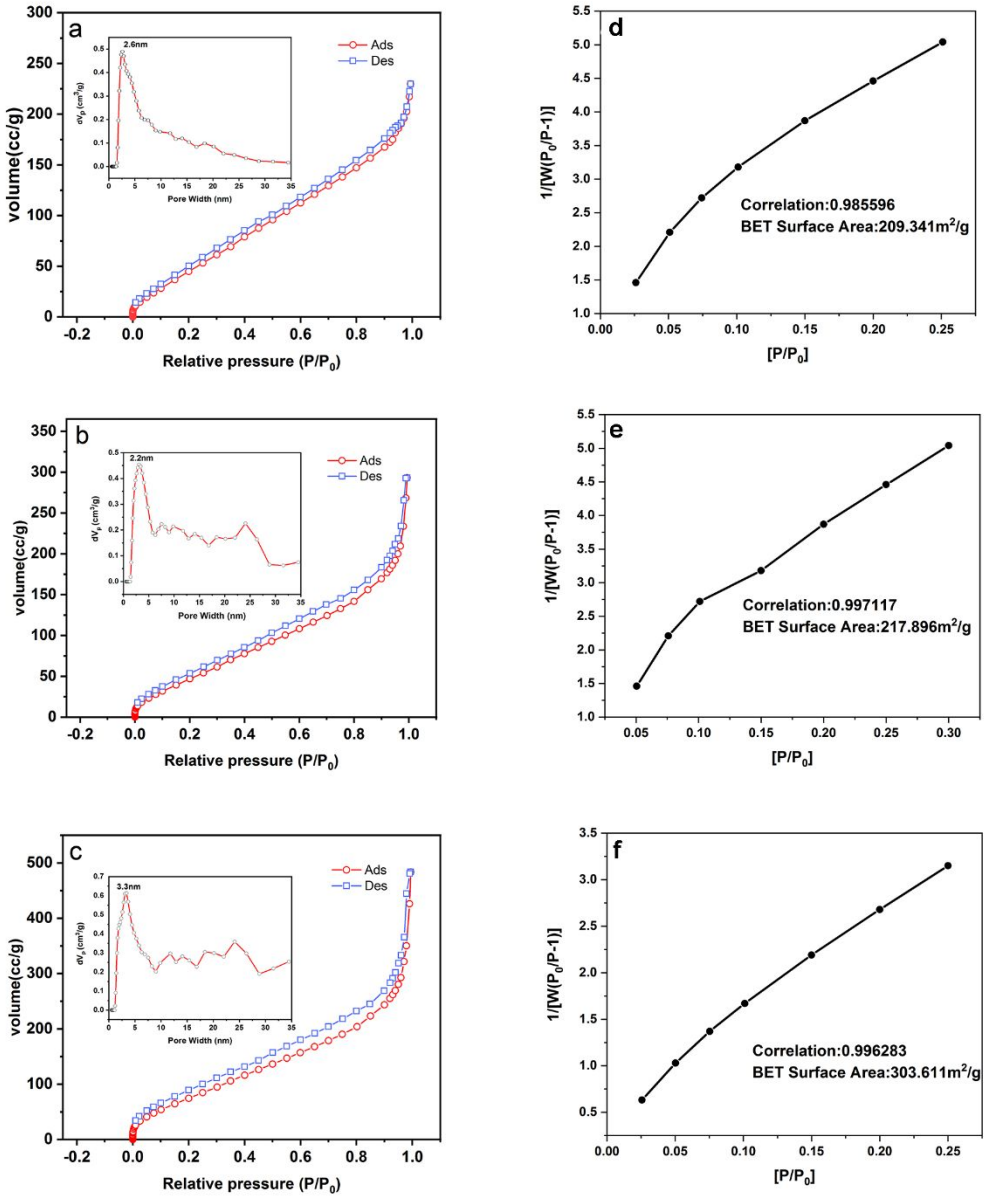

Figure S2. N_2 adsorption and desorption isotherms of CCOFs. (a) COF-TpgDB, (b) COF-TpgBD, (c) COF-TpgTd. BET surface area curves for CCOFs calculated from the isotherm. (d) COF-TpgDB, (e) COF-TpgBD, (f) COF-TpgTd.

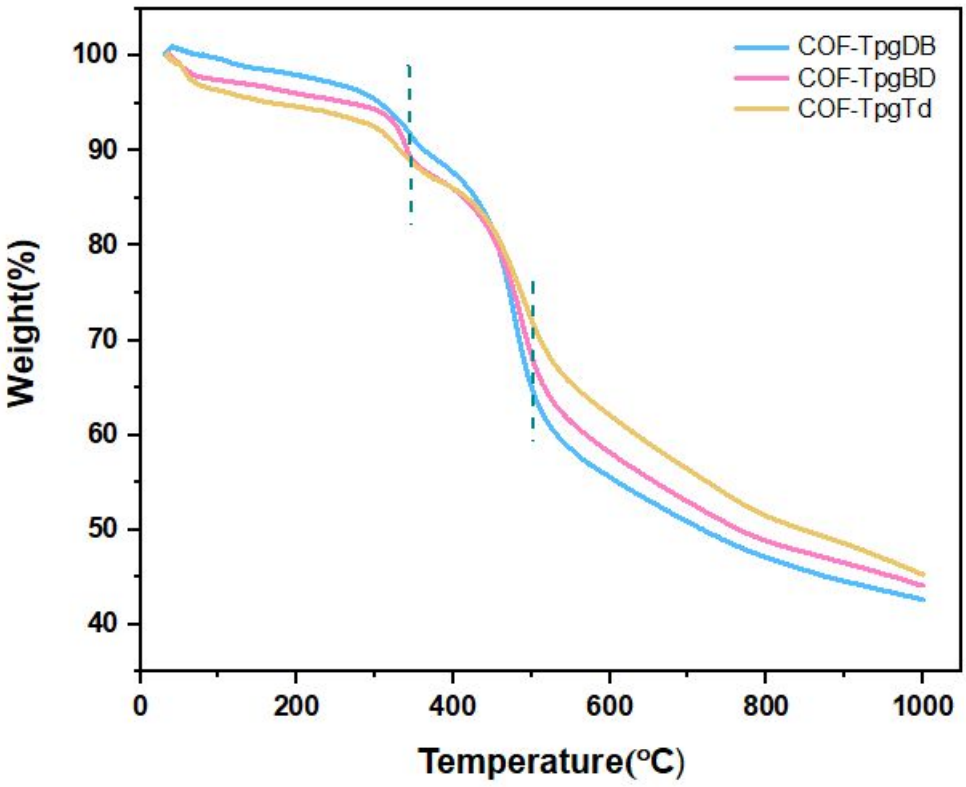

Figure S3. Thermogravimetric analysis curve of COFs (a, blue) COF-TpgDB, (b, pink) COF-TpgBD, and (c, orange) COF-TpgTd.

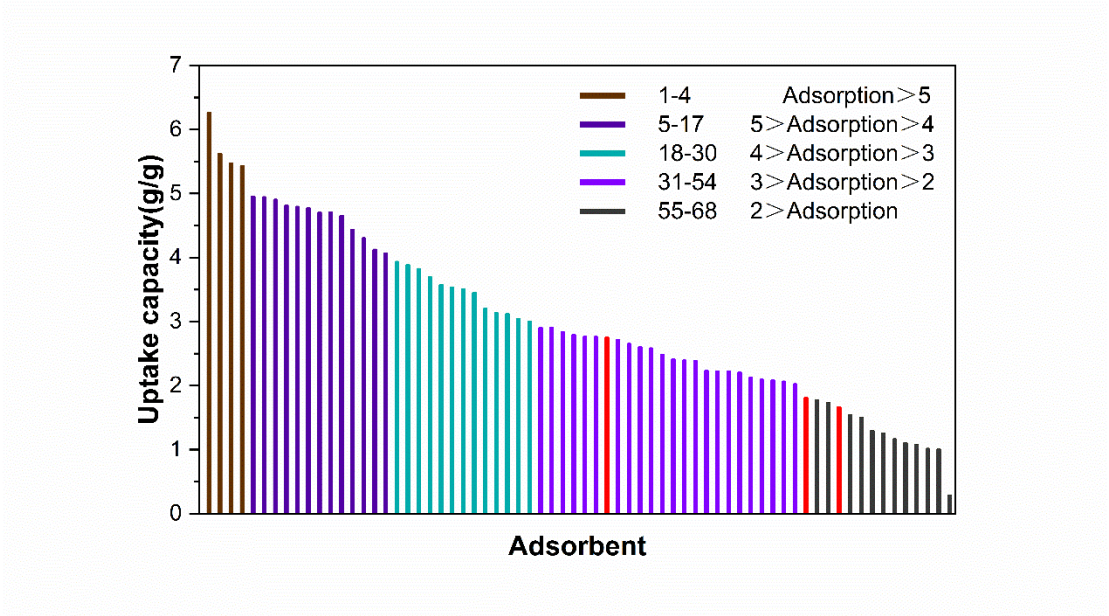

Figure S4. Iodine uptake of different adsorbents. The red bars represent the 2D COFs in this work.

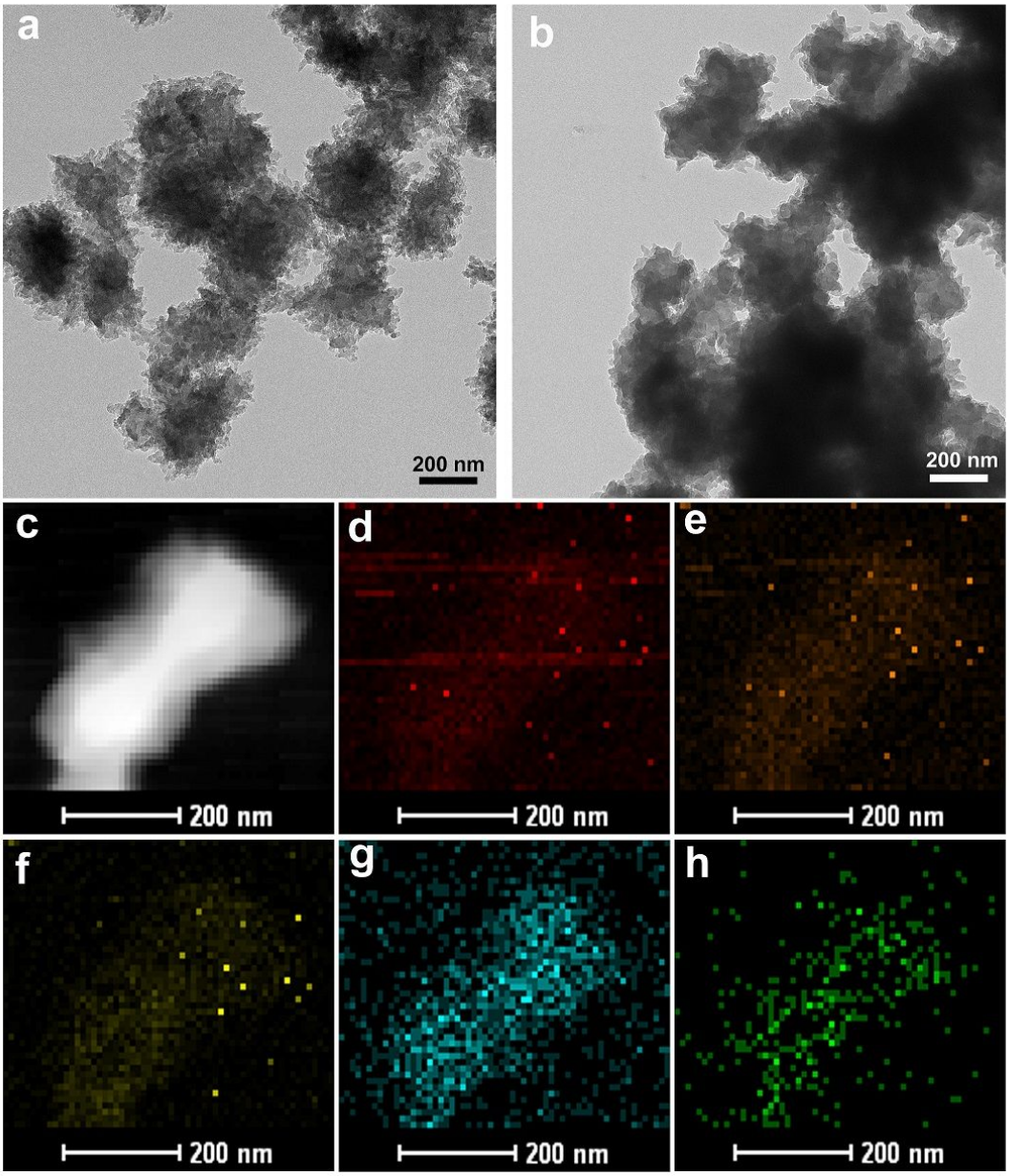

Figure S5. TEM images of (a) pristine COF-TpgDB; (b) iodine-laden COF-TpgDB; (c) HAADF-STEM of iodine-laden COF-TpgDB; (d) C-K elemental mapping images of iodine-laden COF-TpgDB; (e) N-K elemental mapping images of iodine-laden COF-TpgDB; (f) O-K elemental mapping images of iodine-laden COF-TpgDB; (g) I-L elemental mapping images of iodine-laden COF-TpgDB; (h) I-K elemental mapping images of iodine-laden COF-TpgDB.

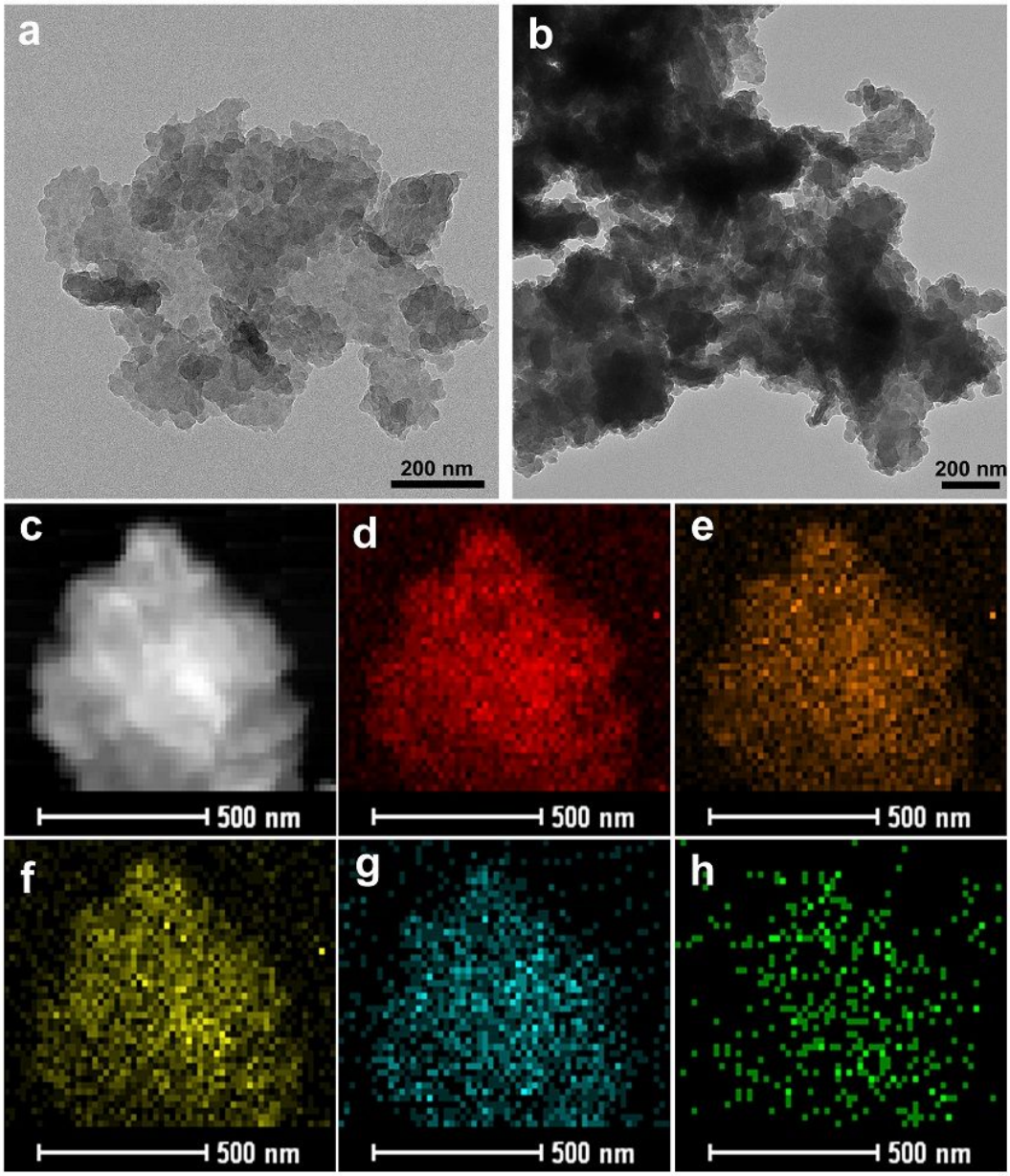

Figure S6. TEM images of (a) pristine COF-TpgBD; (b) iodine-laden COF-TpgBD; (c) HAADF-STEM of iodine-laden COF-TpgBD; (d) C-K elemental mapping images of iodine-laden COF-TpgBD; (e) N-K elemental mapping images of iodine-laden COF-TpgBD; (f) O-K elemental mapping images of iodine-laden COF-TpgBD; (g) I-L elemental mapping images of iodine-laden

COF-TpgBD; (h) I-K elemental mapping images of iodine-laden COF-TpgBD.

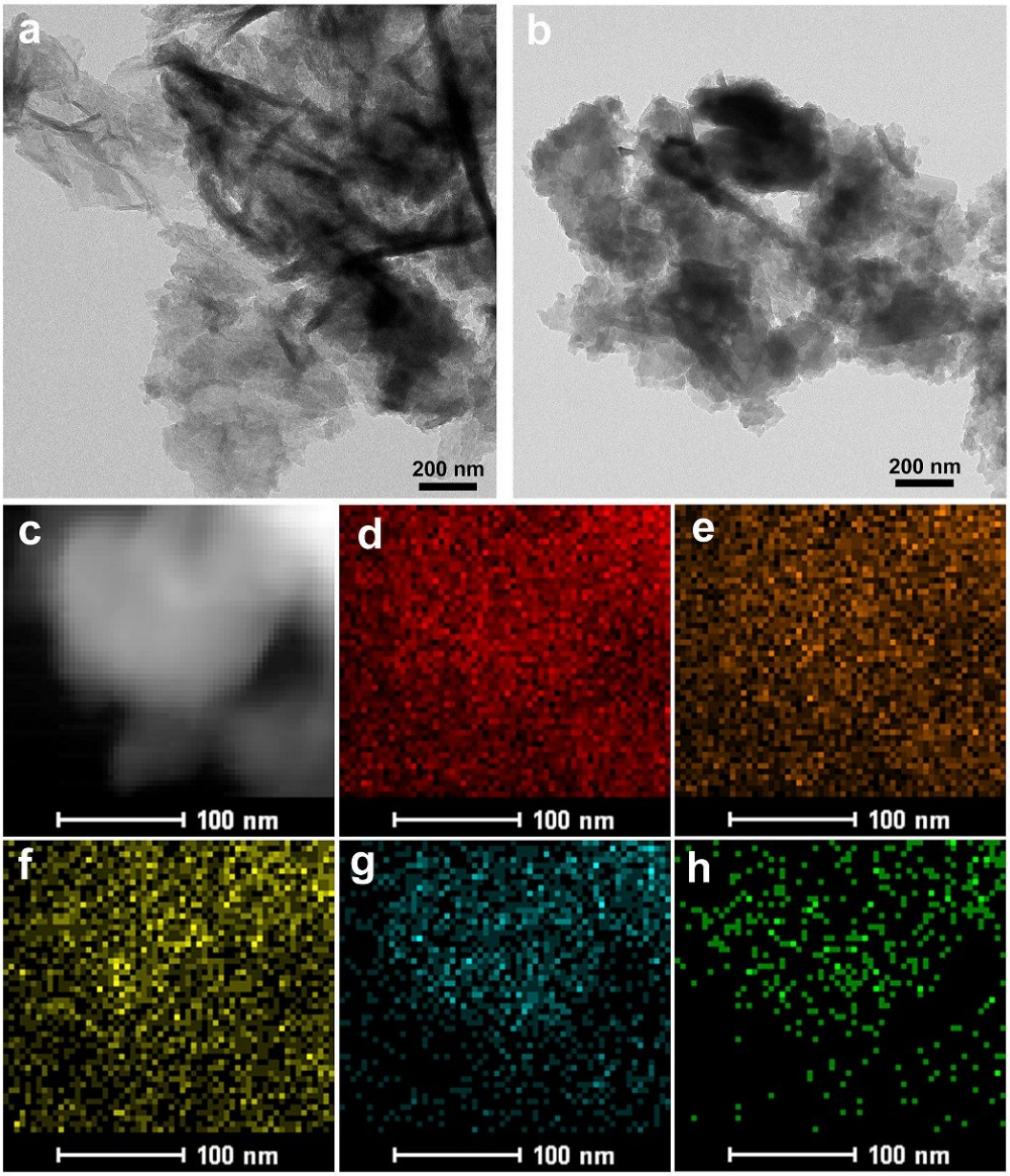

Figure S7. TEM images of (a) pristine COF-TpgTd; (b) iodine-laden COF-TpgTd; (c) HAADF-STEM of iodine-laden COF-TpgTd; (d) C-K elemental mapping images of iodine-laden COF-TpgTd; (e) N-K elemental mapping

images of iodine-laden COF-TpgTd; (f) O-K elemental mapping images of iodine-laden COF-TpgTd; (g) I-L elemental mapping images of iodine-laden COF-TpgTd; (h) I-K elemental mapping images of iodine-laden COF-TpgTd.

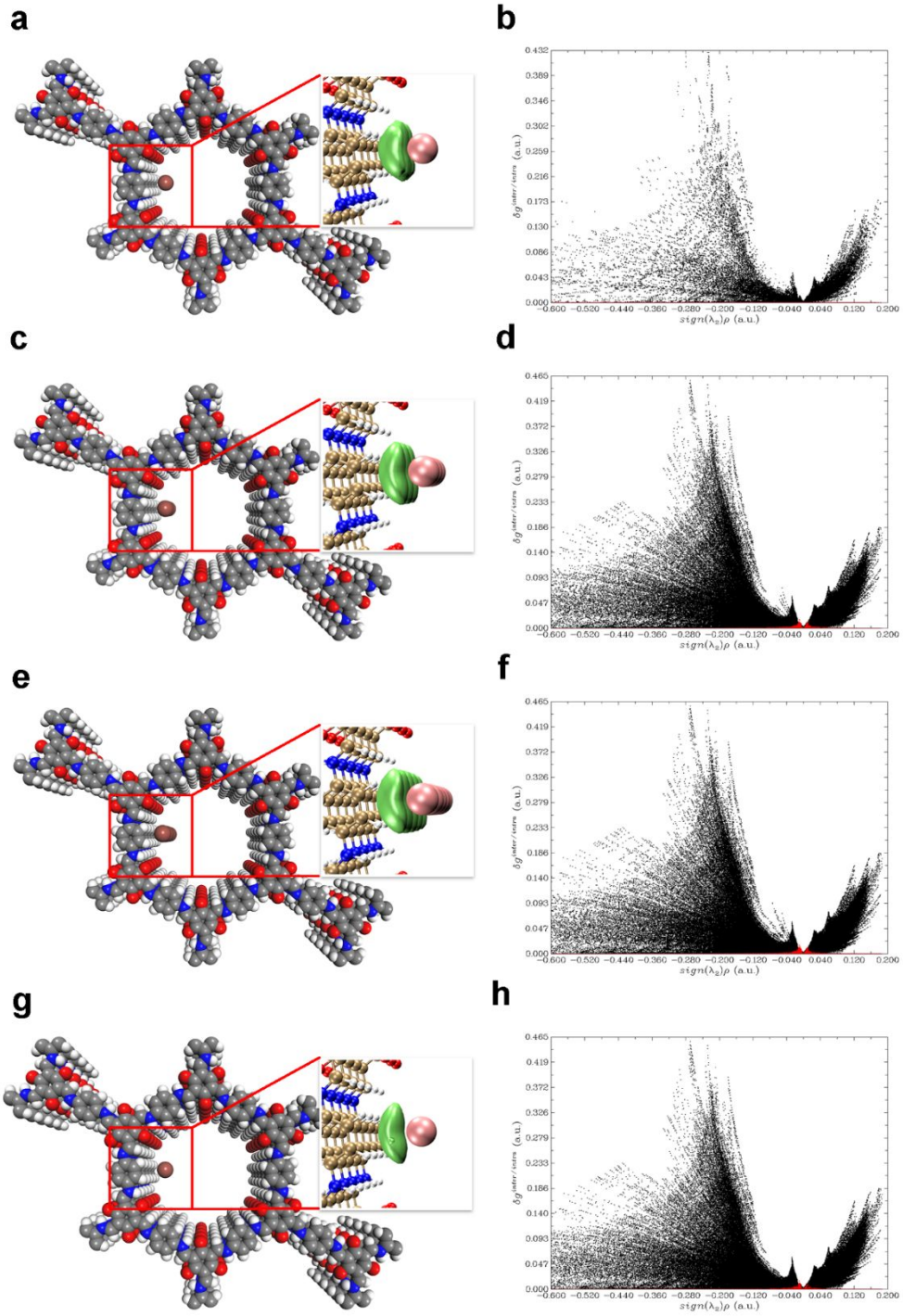

Figure S8. Simulated characterization of the iodine species capturing sites (diamine linker, DB) and IGM Scatter plot of COF-TpgDB. (a, b) I_2; (c, d) I_3^-; (e, f) I_5^-; (g, h) I^+.

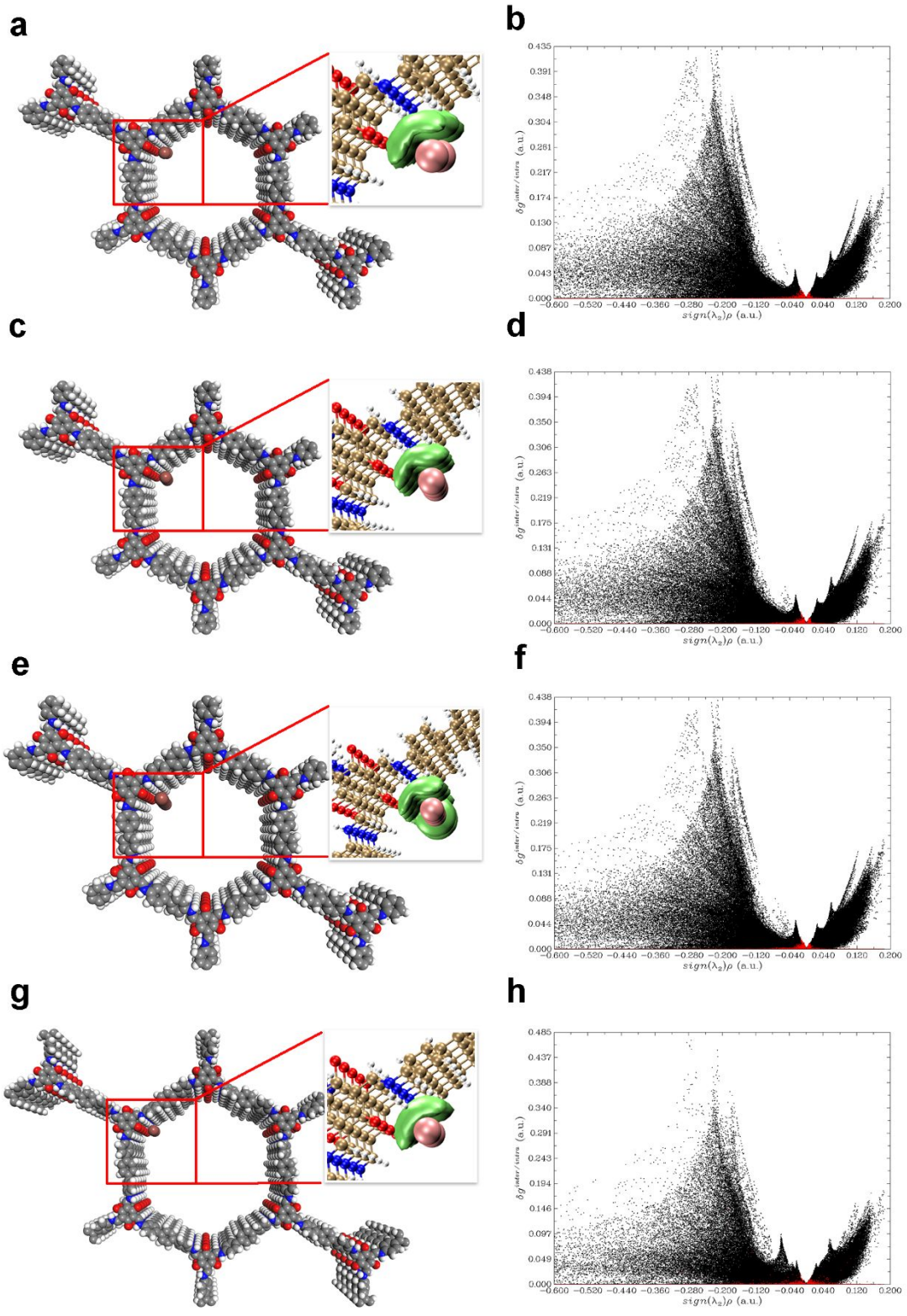

Figure S9. Simulated characterization of the iodine species capturing sites (Tpg) and IGM Scatter plot of COF-TpgBD. (a, b) I_2; (c, d) I_3^-; (e, f) I_5^-; (g, h) I^+.

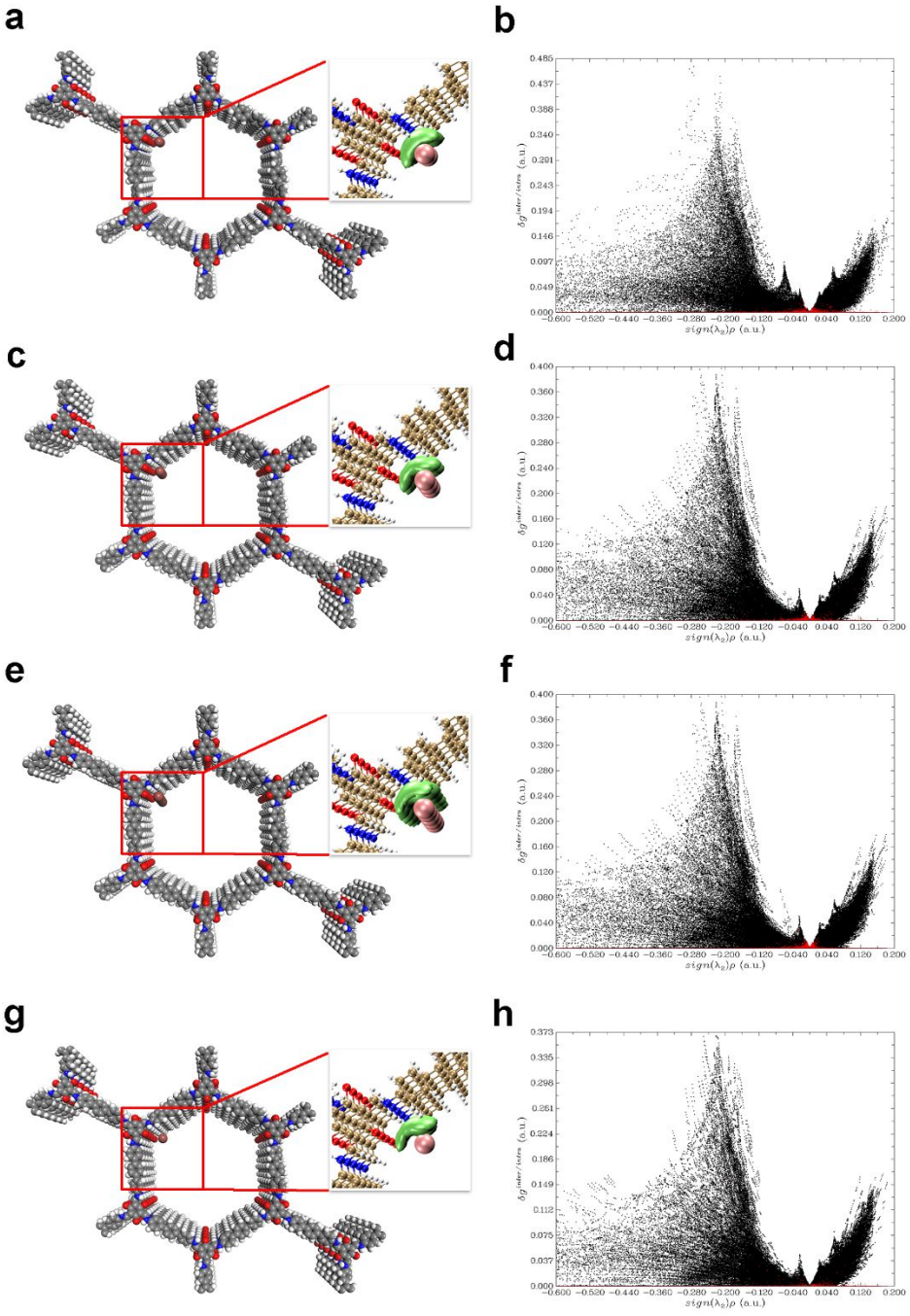

Figure S10. Simulated characterization of the iodine species capturing sites (diamine linker, DB) and IGM Scatter plot of COF-TpgBD. (a, b) I_2; (c, d) I_3^-; (e, f) I_5^-; (g, h) I^+.

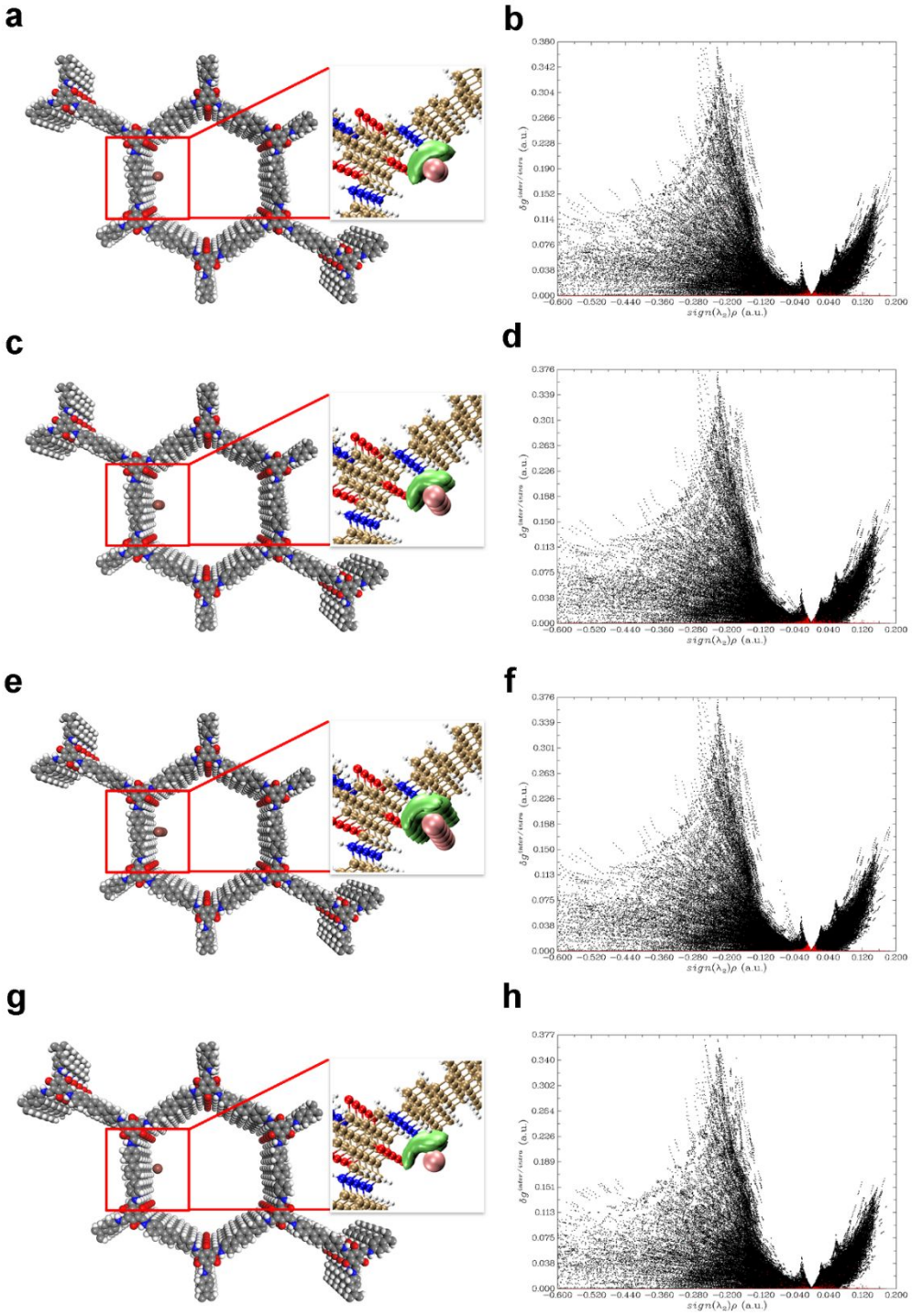

Figure S11. Simulated characterization of the iodine species capturing sites (Tpg) and IGM Scatter plot of COF-TpgBD. (a, b) I_2; (c, d) I_3^-; (e, f) I_5^-; (g, h) I^+.

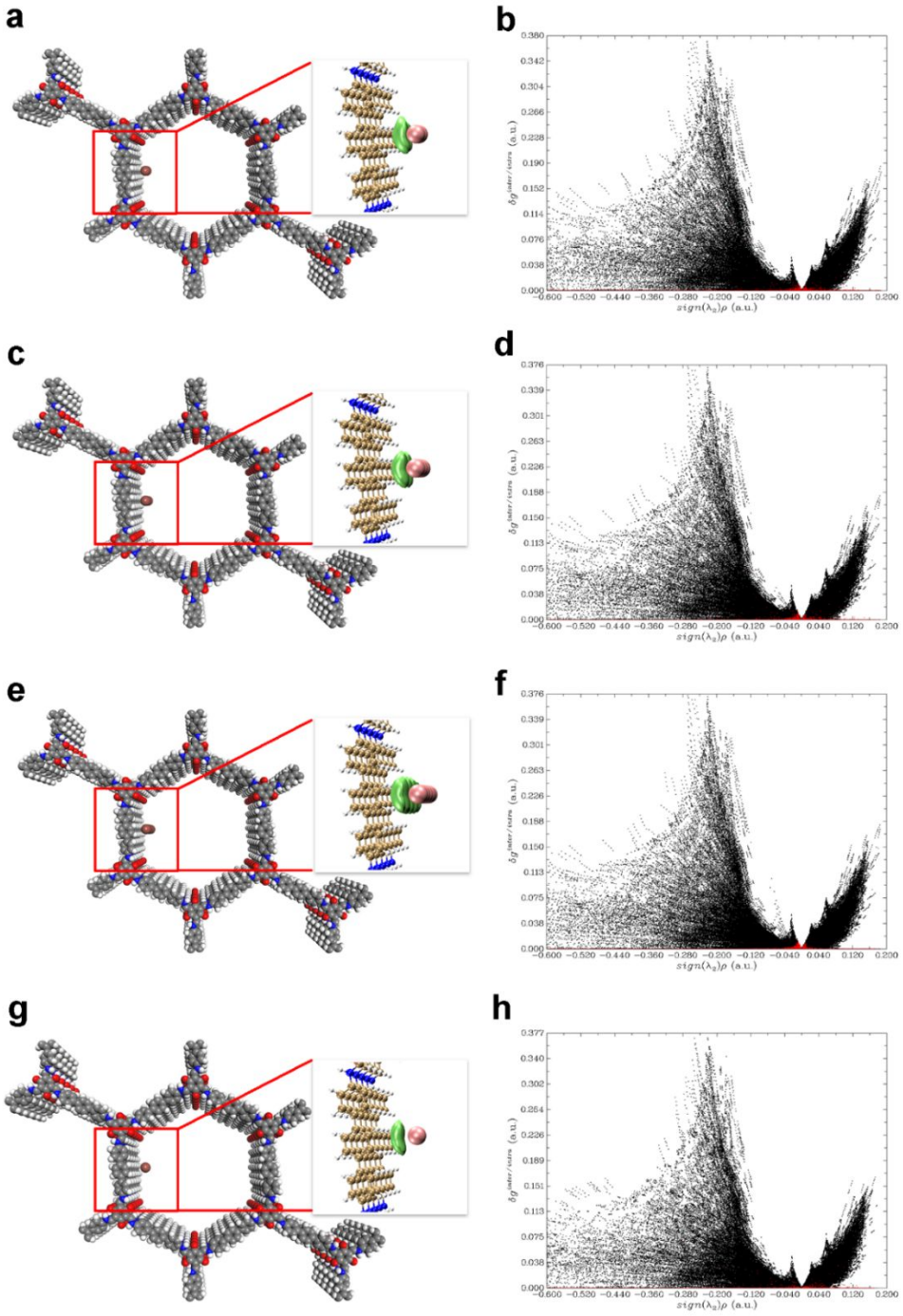

Figure S12. Simulated characterization of the iodine species capturing sites (Tpg) and IGM Scatter plot of CCOFs. (a, b) I_2; (c, d) I_3^-; (e, f) I_5^-; (g, h) I^+.

Table S1. The pore properties of COF-TpgDB, COF-TpgBD and COF-TpgTd

sample	S_{BET}/m^2g^{-1}	proe size/nm	pore volume/ccg^{-1}
COF-TpgDB	209.6	6.8	0.36
COF-TpgBD	217.9	8.3	0.46
COF-TpgTd	303.6	9.9	0.75

Table S2 Iodine uptake of different adsorbents

Adsorbent	Iodine uptake (g/g)	Ref.	Adsorbent	Iodine uptake (g/g)	Ref.
TPB-DMTP	6.26	1	PAF-24	2.76	20
TJNU-201	5.62	2	TTA-TFB	2.76	1
BTT-TAPT	5.47	3	COF-TpgDB	2.75	-
TPT-BD-COF	5.43	4	PAF-23	2.71	20
TTA-TTB	4.95	1	NAPOP-4	2.65	21
P-TzTz	4.94	5	PAF-25	2.6	20
TTPPA	4.9	6	$COP2^{++}$	2.58	22
SIOC-COF-7	4.81	7	$CalP_3\_Li$	2.48	9
ETTA-TPA	4.79	8	NAPOP-3	2.41	21
CalPOF-1	4.77	9	NAPOP-2	2.39	21
COF-DL229	4.7	10	Azo-Trip	2.38	23
ETTA-TPA	4.7	8	BDP-CPP-2	2.23	18
$TPT-DHBD_{25}-COF$	4.65	4	SCMP-2	2.22	24
TTPB	4.43	11	NRPP-2	2.22	25
$TPT-DHBD_{50}-COF$	4.3	4	CalP4	2.2	9

TPT-DHBD$_{75}$-COF	4.12	4	COP1^{++}	2.12	22
CalPOFs	4.06	12	FCMP-600-2	2.09	26
TDPDB	3.93	13	CMPN-3	2.08	27
TPT-DHBD-COF	3.88	4	NAPOP-1	2.06	21
POP-2	3.82	14	NiP-CMP	2.02	28
TFBCz-PDA	3.69	1	COF-TpgBD	1.81	-
POP-1	3.57	14	TTPT	1.77	29
CalPOF-3	3.53	9	{[(ZnI$_2$)$_3$(tpt)$_2$]	1.73	30
HCOFs-4	3.5	15	COF-TpgTd	1.66	-
SCMP-II	3.45	16	MFM-300(Sc)	1.54	31
HCOFs-2	3.2	15	HMTI-1	1.5	32
TTDAB	3.13	11	MFM-300(Fe)	1.29	31
CalP4_Li	3.12	9	ZIF-8	1.25	33
Tm-MTDAB	3.04	11	MFM-300(In)	1.16	31
HCOFs-3	3	15	CMPN-2	1.1	27
AzoPPN	2.9	17	Zr$_6$O$_4$(OH)$_4$(sdc)$_6$	1.07	21
HCOF-1	2.9	15	Zn$_3$(DL-lac)$_2$(pybz)$_2$	1.01	34
BDP-CPP-1	2.83	18	HMTI-2	1	30
Zr$_6$O$_4$(OH)$_4$(peb)$_6$	2.79	19	Ag-MOR	0.28	35

Computational Section

The distant of C=O…I_2, >NH…I_2 and the Ph…I_2 of COF-TpgBD and COF-TpgTd are 3.48, 3.78, 3.50, 3.42, 3.62 and 3.41 Å (Figure S9a, S10a, S11a and S12a), respectively. The average δg^{inter} value of I_2 at the Tpg and DB adsorption site of COF-TpgBD and COF-TpgTd are 0.09, 0.07,0.09 and 0.08 (Figure S9b, S10b, S11b and S12b), respectively.

The distant of C=O…I_3^-, >NH…I_3^- and the Ph…I_3^- of COF-TpgBD and COF-

TpgTd are 3.50, 3.04, 3.83, 3.44, 3.22 and 3.71 Å (Figure S9c, S10c, S11c and S12c), respectively. The average δg^{inter} value of I_2 at the Tpg and DB adsorption site of COF-TpgBD and COF-TpgTd are 0.09, 0.12, 0.10 and 0.09 (Figure S9d, S10d, S11d and S12d), respectively.

The distant of C=O…I_5^-, >NH…I_5^- and the Ph…I_5^- of COF-TpgBD and COF-TpgTd are 3.50, 3.05, 3.83, 3.44, 3.24 and 3.71 Å (Figure S9e, S10e, S11e and S12e), respectively. The average δg^{inter} value of I_2 at the Tpg and DB adsorption site of COF-TpgBD and COF-TpgTd are 0.09, 0.12, 0.10 and 0.09 (Figure S9f, S10f, S11f and S12f), respectively.

The distant of C=O…I^+, >NH…I^+ and the Ph…I^+ of COF-TpgBD and COF-TpgTd are 3.33, 3.56, 3.28, 3.43, 3.52 and 3.15 Å (Figure S9g, S10g, S11g and S12g), respectively. The average δg^{inter} value of I_2 at the Tpg and DB adsorption site of COF-TpgBD and COF-TpgTd are 0.10, 0.09, 0.09 and 0.11 (Figure S9h, S10h, S11h and S12h), respectively.

References

1 Wang, P.; Xu, Q.; Li, Z. P.; Jiang, W. M.; Jiang, Q. H.; Jiang, D. L., Exceptional Iodine Capture in 2D Covalent Organic Frameworks. *Adv. Mater.* **2018,** 30 (29).

2. Li, J. H.; Zhang, H. X.; Zhang, L. Y.; Wang, K.; Wang, Z. K.; Liu, G. Y.; Zhao, Y. L.; Zeng, Y. F., Two-dimensional covalent-organic frameworks for ultrahigh iodine capture. *J. Mater. Chem. A*. **2020,** 8 (19), 9523-9527.

3. Pan, X. W.; Qin, X. H.; Zhang, Q. H.; Ge, Y. S.; Ke, H. Z.; Cheng, G. E., N- and S-rich covalent organic framework for highly efficient removal of indigo carmine and reversible iodine capture. *Micropor. Mesopor. Mat.* **2020,** 296.

4. Guo, X. H.; Tian, Y.; Zhang, M. C.; Li, Y.; Wen, R.; Li, X.; Li, X. F.; Xue, Y.; Ma, L. J.; Xia, C. Q.; Li, S. J., Mechanistic Insight into Hydrogen-Bond-Controlled Crystallinity and Adsorption Property of Covalent Organic Frameworks from Flexible Building Blocks. *Chem. Mater.* **2018,** 30 (7), 2299-2308.

5. Pan, X. W.; Ding, C. H.; Zhang, Z. M.; Ke, H. Z.; Cheng, G. E., Functional porous organic polymer with high S and N for reversible iodine capture. *Micropor. Mesopor. Mat.* **2020,** 300.

6. Geng, T. M.; Zhu, Z. M.; Zhang, W. Y.; Wang, Y., A nitrogen-rich fluorescent conjugated microporous polymer with triazine and triphenylamine units for high iodine capture and nitro aromatic compound detection. *J. Mater. Chem. A.* **2017,** 5 (16), 7612-7617.

7. Yin, Z. J.; Xu, S. Q.; Zhan, T. G.; Qi, Q. Y.; Wu, Z. Q.; Zhao, X., Ultrahigh volatile iodine uptake by hollow microspheres formed from a heteropore covalent organic framework. *Chem. Commun.* **2017,** 53 (53), 7266-7269.

8. Ascherl, L.; Sick, T.; Margraf, J. T.; Lapidus, S. H.; Calik, M.; Hettstedt, C.; Karaghiosoff, K.; Doblinger, M.; Clark, T.; Chapman, K. W.; Auras, F.; Bein, T., Molecular docking sites designed for the generation of highly crystalline covalent organic frameworks. *Nat. Chem.* **2016,** 8 (4), 310-316.

9. Shetty, D.; Raya, J.; Han, D. S.; Asfari, Z.; Olsen, J. C.; Trabolsi, A., Lithiated Polycalix[4]arenes for Efficient Adsorption of Iodine from Solution and Vapor Phases. *Chem.*

Mater. **2017,** 29 (21), 8968-8972.

10. Wang, C.; Wang, Y.; Ge, R. L.; Song, X. D.; Xing, X. Q.; Jiang, Q. K.; Lu, H.; Hao, C.; Guo, X. W.; Gao, Y. A.; Jiang, D. L., A 3D Covalent Organic Framework with Exceptionally High Iodine Capture Capability. *Chem-Eur. J.* **2018,** 24 (3), 585-589.

11. Geng, T. M.; Ye, S. N.; Zhu, Z. M.; Zhang, W. Y., Triazine-based conjugated microporous polymers with N,N,N ',N '-tetraphenyl-1,4-phenylenediamine,1,3,5-tris(diphenylamino)benzene and 1,3,5-tris[(3-methylphenyl)-phenylamino]benzene as the core for high iodine capture and fluorescence sensing of o-nitrophenol. *J. Mater. Chem. A.* **2018,** 6 (6), 2808-2816.

12. Su, K. Z.; Wang, W. J.; Li, B. B.; Yuan, D. Q., Azo-Bridged Calix[4]resorcinarene-Based Porous Organic Frameworks with Highly Efficient Enrichment of Volatile Iodine. Acs. Sustain. *Chem. Eng*. **2018,** 6 (12), 17402-17409.

13. Geng, T. M.; Liu, M.; Zhang, C.; Hu, C.; Xia, H. Y., The preparation of covalent triazine-based framework via Friedel-Crafts reaction of 2,4,6-trichloro-1,3,5-triazine with N,N '-diphenyl-N,N '-di(m-tolyl)benzidine for capturing and sensing to iodine. *Polym. Advan. Technol.* **2020,** 31 (6), 1388-1394.

14. Qian, X.; Wang, B.; Zhu, Z. Q.; Sun, H. X.; Ren, F.; Mu, P.; Ma, C. H.; Liang, W. D.; Li, A., Novel N-rich porous organic polymers with extremely high uptake for capture and reversible storage of volatile iodine. *J. Hazard. Mater.* **2017,** 338, 224-232.

15. Jiang, X. F.; Cui, X. Z.; Duncan, A. J. E.; Li, L.; Hughes, R. P.; Staples, R. J.; Alexandrov, E. V.; Proserpio, D. M.; Wu, Y. Y.; Ke, C. F., Topochemical Synthesis of Single-Crystalline Hydrogen-Bonded Cross-Linked Organic Frameworks and Their Guest-Induced

Elastic Expansion. *J. Am. Chem. Soc.* **2019,** 141 (27), 10915-10923.

16. Qian, X.; Zhu, Z. Q.; Sun, H. X.; Ren, F.; Mu, P.; Liang, W. D.; Chen, L. H.; Li, A., Capture and Reversible Storage of Volatile Iodine by Novel Conjugated Microporous Polymers Containing Thiophene Units. *Acs. Appl. Mater. Inter.* **2016,** 8 (32), 21063-21069.

17. Li, H.; Ding, X. S.; Han, B. H., Porous Azo-Bridged Porphyrin-Phthalocyanine Network with High Iodine Capture Capability. *Chem-Eur. J.* **2016,** 22 (33), 11863-11868.

18. Zhu, Y. L.; Ji, Y. J.; Wang, D. G.; Zhang, Y.; Tang, H.; Jia, X. R.; Song, M.; Yu, G. P.; Kuang, G. C., BODIPY-based conjugated porous polymers for highly efficient volatile iodine capture. *J. Mater. Chem. A.* **2017,** 5 (14), 6622-6629.

19. Marshall, R. J.; Griffin, S. L.; Wilson, C.; Forgan, R. S., Stereoselective Halogenation of Integral Unsaturated C-C Bonds in Chemically and Mechanically Robust Zr and Hf MOFs. *Chem-Eur. J.* **2016,** 22 (14), 4870-4877.

20. Yan, Z. J.; Yuan, Y.; Tian, Y. Y.; Zhang, D. M.; Zhu, G. S., Highly Efficient Enrichment of Volatile Iodine by Charged Porous Aromatic Frameworks with Three Sorption Sites. Angew. *Chem. Int. Edit.* **2015,** 54 (43), 12733-12737.

21. Weng, J. Y.; Xu, Y. L.; Song, W. C.; Zhang, Y. H., Tuning the Adsorption and Fluorescence Properties of Aminal-Linked Porous Organic Polymers through N-Heterocyclic Group Decoration. *J. Polym. Sci. Pol. Chem.* **2016,** 54 (12), 1724-1730.

22. Das, G.; Prakasam, T.; Nuryyeva, S.; Han, D. S.; Abdel-Wahab, A.; Olsen, J. C.; Polychronopoulou, K.; Platasiglesias, C.; Ravaux, F.; Jouiad, M.; Trabolsi, A., Multifunctional redox-tuned viologen-based covalent organic polymers. *J. Mater. Chem. A.* **2016,** 4 (40), 15361-15369.

23. Dang, Q. Q.; Wang, X. M.; Zhan, Y. F.; Zhang, X. M., An azo-linked porous triptycene network as an absorbent for CO2 and iodine uptake. *Polym Chem-Uk.* **2016,** 7 (3), 643-647.

24. Ren, F.; Zhu, Z. Q.; Qian, X.; Liang, W. D.; Mu, P.; Sun, H. X.; Liu, J. H.; Li, A., Novel thiophene-bearing conjugated microporous polymer honeycomb-like porous spheres with ultrahigh iodine uptake. *Chem. Commun.* **2016,** 52 (63), 9797-9800.

25. Abdelmoaty, Y. H.; Tessema, T. D.; Choudhury, F. A.; El-Kadri, O. M.; El-Kaderi, H. M., Nitrogen-Rich Porous Polymers for Carbon Dioxide and Iodine Sequestration for Environmental Remediation. *Acs. Appl. Mater. Inter*. **2018,** 10 (18), 16049-16058.

26. Li, G. Y.; Yao, C.; Wang, J. K.; Xu, Y. H., Synthesis of tunable porosity of fluorine-enriched porous organic polymer materials with excellent CO2, CH4 and iodine adsorption. *Sci. Rep-Uk* **2017,** 7.

27. Shi, Q.; Sun, H. X.; Yang, R. X.; Zhu, Z. Q.; Liang, W. D.; Tan, D. Z.; Yang, B. P.; Li, A.; Deng, W. Q., Synthesis of conjugated microporous polymers for gas storage and selective adsorption. *J. Mater. Sci.* **2015,** 50 (19), 6388-6394.

28. Sigen, A.; Zhang, Y. W.; Li, Z. P.; Xia, H.; Xue, M.; Liu, X. M.; Mu, Y., Highly efficient and reversible iodine capture using a metalloporphyrin-based conjugated microporous polymer. *Chem. Commun.* **2014,** 50 (62), 8495-8498.

29. Geng, T. M.; Zhang, W. Y.; Zhu, Z. M.; Chen, G. F.; Ma, L. Z.; Ye, S. N.; Niu, Q. Y., A covalent triazine-based framework from tetraphenylthiophene and 2,4,6-trichloro-1,3,5-triazine motifs for sensing o-nitrophenol and effective I-2 uptake. Polym Chem-Uk **2018,** 9 (6), 777-784.

30. Brunet, G.; Safin, D. A.; Aghaji, M. Z.; Robeyns, K.; Korobkov, I.; Woo, T. K.;

Murugesu, M., Stepwise crystallographic visualization of dynamic guest binding in a nanoporous framework. *Chem. Sci.* **2017,** 8 (4), 3171-3177.

31. Zhang, X. R.; da Silva, I.; Godfrey, H. G. W.; Callear, S. K.; Sapchenko, S. A.; Cheng, Y. Q.; Vitorica-Yrezabal, I.; Frogley, M. D.; Cinque, G.; Tang, C. C.; Giacobbe, C.; Dejoie, C.; Rudic, S.; Ramirez-Cuesta, A. J.; Denecke, M. A.; Yang, S. H.; Schroder, M., Confinement of Iodine Molecules into Triple-Helical Chains within Robust Metal-Organic Frameworks. *J. Am. Chem. Soc*. **2017,** 139 (45), 16289-16296.

32. Hashemi, L.; Morsali, A., Reversible crystal-to-crystal transformation in nano-porous three-dimensional lead(II) MOFs; study of solvent attendance on iodide adsorption affinity. *Crystengcomm.* **2012,** 14 (24), 8349-8351.

33. Sava, D. F.; Rodriguez, M. A.; Chapman, K. W.; Chupas, P. J.; Greathouse, J. A.; Crozier, P. S.; Nenoff, T. M., Capture of Volatile Iodine, a Gaseous Fission Product, by Zeolitic Imidazolate Framework-8. *J. Am. Chem. Soc*. **2011,** 133 (32), 12398-12401.

34. Zeng, M. H.; Wang, Q. X.; Tan, Y. X.; Hu, S.; Zhao, H. X.; Long, L. S.; Kurmoo, M., Rigid Pillars and Double Walls in a Porous Metal-Organic Framework: Single-Crystal to Single-Crystal, Controlled Uptake and Release of Iodine and Electrical Conductivity. *J. Am. Chem. Soc*. **2010,** 132 (8), 2561.

35 Ru-Xin, Yao, Xin. A Luminescent Zinc(II) Metal-Organic Framework (MOF) with Conjugated π -Electron Ligand for High Iodine Capture and Nitro-Explosive Detection.*J. Inorganic Chemistry*, 2016.